Recognition Method of Metal Material Pitting Defect Based on Visual Signal Processing

Ying Zhao(✉) and Li Zhang

Nanchang Institute of Technology, Nanchang 330108, Jiangxi, China

Abstract. Aiming at the problem of large recognition errors in traditional metal material pitting defect recognition methods, this research aims to improve the recognition performance of metal material pitting defects, and proposes a metal material pitting defect recognition method based on visual signal processing. The rail material parameters are set according to the schematic diagram of the U71Mn rail imitation, and the defective metal material imitation model is constructed according to the distribution position of each crack of the U71Mn rail, and then the optical signal of the metal material pitting defect is collected according to the geometric model imaged by the camera. The image of metal material pitting defects undergoes visual signal processing to extract the details of the image in different directions and scales. Based on this, the Mallet algorithm is used to decompose the image of metal material pitting corrosion defects, and the low-frequency components and high-dimensional components of multiple resolutions and multiple features are obtained, and specific fusion rules are selected to select the components of each layer obtained by decomposition, and then wavelet Inverse transformation, complete the fusion and analysis of visual signals of pitting defects in metal materials. Experimental results show that the recognition method of metal material pitting defects based on visual signal processing has high recognition performance.

Keywords: Visual signal processing · Metal materials · Pitting defect recognition · High dimensional component

1 Introduction

Pitting defects will directly affect the service performance and service life of metal materials. It is of great significance to carry out effective non-destructive testing and evaluation to provide data support for fatigue life prediction [1]. Metal material structure changes state and forms new phase under the action of medium, which leads to corrosion damage. Corrosion damage is very serious to national economy and national defense construction. It will not only lead to production stoppage, material structure failure, resource loss, hazardous material leakage, but also lead to significant economic losses and even catastrophic consequences. According to statistics, the amount of metal scrapped due to corrosion is equivalent to 20%–40% of the annual metal production in the world. The annual average cost of solving corrosion damage in developed countries accounts

W. Fu et al. (Eds.): ICMTEL 2021, LNICST 387, pp. 14–26, 2021.
https://doi.org/10.1007/978-3-030-82562-1_2

for 2%–4% of the national economy, and is increasing year by year. Every year, many countries in the world have to invest a lot of manpower and material resources for corrosion detection and protection. Corrosion detection has become one of the important fields of modern science and technology research. It is of great significance for the safety and economy of metal materials and structures to find and evaluate the corrosion damage timely and accurately.

Pitting corrosion is the initial stage of corrosion damage. Because the metal surface is under tensile stress or chemical substances, the protective layer is damaged and local penetration occurs, so that the metal matrix is directly exposed to the corrosive environment to form local corrosion pores. A form of corrosion damage developed in depth. The occurrence and expansion of pitting corrosion can be divided into two stages, namely pitting nucleation and growth [2, 3]. There are two theories about the causes of pitting corrosion: one is that pitting occurs when the oxygen adsorption point on the metal surface is replaced by chloride ions; the other is that the radius of chloride ions is small and can pass through the passivation film and enter the film. The generated conductive induced ions cause the membrane to maintain a high current density at a specific point, causing the cations to move randomly. When the electric field at the membrane-solution interface reaches a certain critical value, pitting corrosion occurs. After the pitting nucleus is formed, it will continue to grow, and when it reaches a critical size, macroscopic pits will appear. There are many theories about the expansion mechanism of pits, and a well-recognized theory is that the process of autocatalytic occlusion of batteries occurs in pits.

The location of pitting corrosion has strong randomness, and it is easy to form fatigue source in pitting area. Pitting corrosion forms corrosion pits on the surface of the structure, which changes the surface state of the structure, and then leads to local or comprehensive damage. It depends on the comprehensive influence of pitting pit depth, stress level and material fatigue crack. In the interaction between pitting and fatigue, pitting is generally regarded as a surface crack, and the crack growth rate is controlled by the pitting kinetics. When the pitting corrosion grows to the critical size or the fatigue crack growth rate exceeds the pitting corrosion growth rate, fatigue cracks will be initiated at the pitting pit. The fatigue crack nucleates at the pitting pit, then goes through the pitting growth, the transition stage from pitting to fatigue crack formation, the short crack propagation, the long crack propagation and the metal structure damage. Sun Mingjian [4] et al. proposed a non-destructive detection method for metal material defects based on multi-modal signals in view of the single modal signal mode and limited detection range of the existing non-destructive testing technology. This method is based on the photoacoustic nondestructive testing method. First, the finite element method is used to analyze the effect of defects on the laser energy absorption and photoacoustic surface wave propagation, and a defect detection method based on the laser absorption and photoacoustic surface wave is proposed; The multi-modal signal detection platform collects the optical, photoacoustic and ultrasonic signals of the defect, and detects the width and distribution information of the crack, as well as the depth and internal extension; In order to improve the recognition rate of packaging printing defects, Liyan S [5] designed a printing defect detection method based on machine vision. Based on the analysis of common defect types, a detection system is built by using digital signal processor

TMS320DM642, and the process of packaging defect detection is discussed. Based on this, the traditional wavelet transform is improved, which can enhance the image feature information and improve the recognition rate. At the same time, several defect feature extraction methods, including roundness, aspect ratio and gray standard deviation, are presented. Yang Chenlong [6] and others used the recursive analysis method to analyze the detection signal in order to effectively identify the micro defect echo in the ultrasonic testing signal of metal materials. By modeling the ultrasonic backscattering signal. In the ultrasonic testing signal, the echo signal of defect will affect the recursive characteristic of the system. The backscatter signal and defect free backscatter signal of 120 mm diameter low carbon steel bar with 0.8 mm flat bottom hole artificial simulated defects were studied by using recursive analysis. The part of backscattered signal in the test signal of the test block is intercepted, and the recursive analysis is carried out through reasonable parameter selection, and the recursive diagram is drawn. Compared with the recursive image of defect free signal collected by experiment, it is found that the defect signal will produce obvious white cross stripe in the recursive image. Recursive quantitative analysis is used to further study the recursive characteristics of the backscattered signal with defects. The results show that the acquisition time (TT), determination rate (DET) and recursive entropy (entr) are sensitive to the defect signal, and there are obvious peaks at the defect position.

Based on the above background, this paper applies visual signal processing to metal material pitting defect identification, and designs a metal material pitting defect identification method based on visual signal processing. Based on the distribution location of rail cracks, the model of metal material with defects was constructed. Then, the optical signals of metal material pitting defects were collected, and the details of images in different directions and scales were extracted through the signal processing process. Based on this, Mallet algorithm is used to decompose the image of metal material pitting defects, and specific fusion rules are selected to select each layer component obtained by decomposition. Then, through inverse wavelet transformation, the fusion and analysis of visual signals of metal material pitting defects are completed, so as to improve the performance of metal material pitting defect identification. The experimental results show that this method has high recognition performance.

2 Design of Metal Material Pitting Defect Identification Method

2.1 Construction of Metal Model with Defects

A section of U71Mn rail as shown in Fig. 1 was selected as the imitation body. This type of rail is widely used in my country's railway tracks at present, and it is of great significance to use it as an imitation body for research. The material parameters of this type of rail are shown in Table 1. Seven longitudinal cracks were processed on the rail head. The distribution position of each crack is shown in Fig. 2, and the size is shown in Table 2. The shallower rail head cracks 1, 2, 3, and 7 are used to represent defects in the superficial layer, while the deeper cracks 4, 5, and 6 represent defects that penetrate the surface, the superficial layer and the interior.

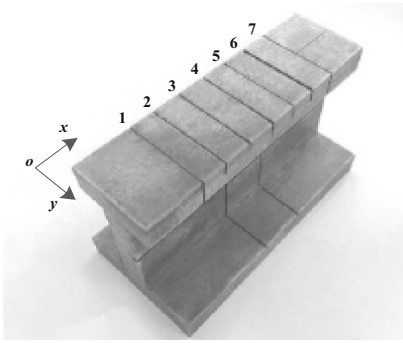

Fig. 1. Schematic diagram of U71Mn rail

Table 1. Rail material parameters

Attributes	Value	Attributes	Value
Density	7850 kg/m	Elastic modulus	$2.1*10^{11}$Pa
Thermal conductivity	45W/(m·K)	Poisson's ratio	0.3
Specific heat capacity	460J(kg·K)	Thermal expansion coefficient	1*10–5

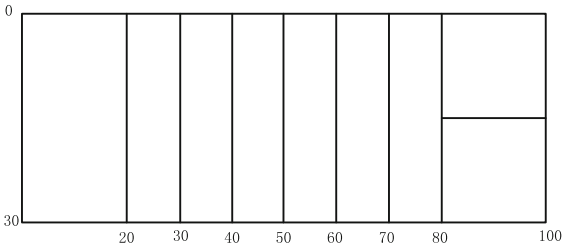

Fig. 2. The distribution position of each crack in U71Mn rail

According to the simulation diagram of U71Mn rail, the material parameters of rail are set, and the simulation model of metal material with defects is constructed by using the distribution position of cracks in U71Mn rail.

2.2 Collect Optical Signals of Pitting Defects in Metal Materials

Camera distortion will affect the accuracy of metal material pitting defect recognition, and the camera calibration can achieve the effect of eliminating distortion. Therefore, before using the camera to collect the image of the phantom, first calibrate it. Camera calibration is actually the process of solving the corresponding relationship between the three-dimensional space position of a point in the camera model and the position of the point in the pixel coordinate system [7–9]. The camera model includes four coordinate systems: world coordinate system, camera coordinate system, image plane coordinate

Table 2. The size of the crack on the imitation body

Numbering	Width (mm)	Depth (mm)
1	0.5	0.5
2	0.5	1.5
3	0.5	1.0
4	0.5	5.5
5	0.5	5.0
6	0.5	5.0
7	0.5	0.5

system and pixel coordinate system, as shown in Fig. 3. The corresponding relations of the four coordinate systems are analyzed below.

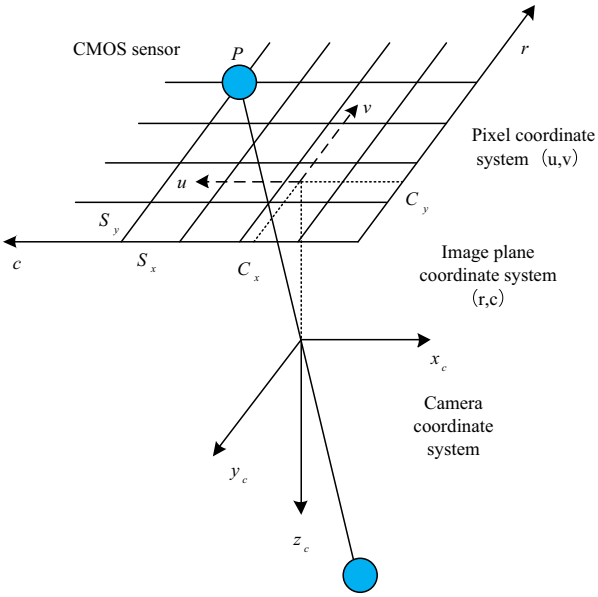

Fig. 3. Geometric model of camera imaging

The transformation relationship between point P_w in the world coordinate system and point P_c in the camera coordinate system is as follows:

$$\begin{bmatrix} x_c \\ y_c \\ z_c \end{bmatrix} = R \begin{bmatrix} x_w \\ y_w \\ z_w \end{bmatrix} + T \tag{1}$$

Among them, $T = (t_x, t_y, t_z)$ and $R = R(r_\alpha, r_\rho, r_y)$ respectively represent the translation and rotation process when the world coordinate system is converted to the camera coordinate system.

The projection relationship between point P_c and point P in the plane coordinate system of the pitting defect image of metallic materials is:

$$\frac{u}{v} = \frac{f_c}{z_c} \cdot \frac{x_c}{y_c} \tag{2}$$

Where f_c is the main distance of the camera, that is, the distance between the imaging plane and the projection center, and f_c is parallel to the main axis. The line between the point in the world coordinate system and the projection point in the imaging plane originally passes through the optical center of the camera. However, the lens distortion produces a change that can be approximated as radial distortion, so that the corresponding position of P_w in the plane coordinate system of metal material pitting defect image is as follows:

$$\begin{pmatrix} \bar{u} \\ \bar{v} \end{pmatrix} = \frac{2}{1 + \sqrt{1 - 4k(u^2 + v^2)}} \begin{pmatrix} u \\ v \end{pmatrix} \tag{3}$$

In the formula, the parameter k represents the magnitude of radial distortion. If k is a negative number, the state of distortion is barrel distortion; if k is a positive number, the state of distortion is pincushion distortion.

Finally, according to the transformation relationship between $(\bar{u}, \bar{v})$ and pixel coordinate system shown in formula (3), the pixel coordinates corresponding to P_w can be obtained:

$$\begin{pmatrix} r \\ c \end{pmatrix} = \begin{pmatrix} \frac{\bar{v}}{S_y} + C_y \\ \frac{\bar{u}}{S_x} + C_x \end{pmatrix} \tag{4}$$

In formulas (1)–(4), $(t_x, t_x, t_z, r_\alpha, r_\rho, r_y)$ is called the external parameters of the camera, and $(f_c, k, S_x, S_y, C_x, C_y)$ is called the internal parameters of the camera. The process of calibrating the camera is the process of solving these 12 parameters. One tool required for calibration is a calibration board. Commonly used calibration boards include solid circle array patterns and chess array patterns. The size can be selected according to the field of view. In this article, a 50 mm calibration plate with a solid circular array pattern is selected for calibration.

2.3 Fusion and Analysis of Visual Signals of Metal Pitting Defects

The fusion of the visual signals of the pitting defects of metal materials in three different modes can obtain results that cannot be obtained in a single mode, and can also make the results of the single mode detection more accurate and reliable. The photoacoustic and ultrasonic metal material pitting defect images were fused, and complementary and beneficial information were selected from the defect images of the two respectively, and the inaccurate depth detection results in the photoacoustic and ultrasonic longitudinal sections were determined.

Metal material pitting defect image fusion can be divided into pixel level fusion, feature level fusion and decision level fusion according to the order from low to high [10–12]. Pixel level fusion and feature level fusion respectively refer to the fusion according to the corresponding pixels and features of multiple metal material pitting defect images, while decision level fusion is the final decision after classification, recognition and evaluation based on pixel level fusion and feature level fusion. As pixel level metal material pitting defect image fusion directly processes and fuses the data collected by the sensor, retains more original data and provides fine information that the other two fusion methods can not provide. Therefore, this paper studies the pixel level fusion of photoacoustic image and ultrasonic image.

First, visual signal processing must be performed on the image of pitting defects in metal materials. The image of pitting defects in metallic materials can be regarded as a two-dimensional signal, considering that the two-dimensional scale function $\phi(x, y)$ can be separated, namely:

$$\phi(x, y) = \phi(x)\phi(y) \tag{5}$$

Where a is $\phi(x)$ one-dimensional scale function and $\Psi(x)$ is a wavelet function corresponding to $\phi(x)$, i.e.:

$$\Psi(x) = \sum_{k} h_1(x)\phi(2x - k) \tag{6}$$

Then, the three two-dimensional basic wavelets, $\Psi^{(1)}(x, y) = \phi(x)\Psi(y)$, $\Psi^{(2)}(x, y) = \Psi(x)\phi(y)$, and $\Psi^{(3)}(x, y) = \Psi(x)\Psi(y)$, form a filter bank, which extracts the details of the pitting corrosion defect images of metal materials in different directions and scales. Among them, $\Psi^{(1)}(x, y)$ is used to extract the pitting corrosion defect images of metal materials. For details at low horizontal frequency and high vertical frequency, $\Psi^{(2)}(x, y)$ is used to extract details of metal material pitting defect images at high horizontal frequency and low vertical frequency, $\Psi^{(3)}(x, y)$ is used to extract metal material pitting defect images at high horizontal frequency and high vertical frequency Details under frequency.

For the pitting defect image of source metal material $f(m, n)$, let $C_0(m, n) = f(m, n)$, and mallet algorithm decompose it by wavelet:

$$\begin{cases} C_j(m, n) = \frac{1}{2} \sum\limits_{kj=Z} C_{j-1}(k, l)h_{k-2m}h_{l-2n} \\ d_j^1(m, n) = \frac{1}{2} \sum\limits_{kJeZ} C_{j-1}(k, l)h_{k-2m}g_{i-2n} \\ d_j^2(m, n) = \frac{1}{2} \sum\limits_{k,j=Z} C_{j-1}(k, l)g_{k-2m}h_{i-2n} \\ d_j^3(m, n) = \frac{1}{2} \sum\limits_{k/eZ} C_{j-1}(k, l)g_{k-2m}g_{l-2n} \end{cases} \tag{7}$$

Among them, $C_j(m, n)$ represents the low frequency component, $d_j^1(m, n)$ represents the horizontal edge of the pitting defect image of metal material, $d_j^2(m, n)$ represents the vertical edge of the pitting defect image of metal material, $d_j^3(m, n)$ represents the

diagonal edge of the pitting defect image of metal material, and h and g represent filter banks. Corresponding to $\phi(x)$ and $\Psi(x)$ respectively; Z is an integer set, $1 \leq j \leq N$ and N represent the number of decomposition.

After the metal material pitting defect image decomposition is completed, low-frequency components and high-dimensional components with multiple resolutions and features can be obtained. These high-dimensional components are selected according to certain rules. The commonly used fusion rules include: take large value fusion rule, weighted average fusion rule, regional fusion rule, etc.

In this paper, the source metal material pitting defect images a and B are fused into image F. if the fusion rule is used, the mathematical expression is as follows:

$$C(A,B) = \frac{\sum_{m=1}^{M}\sum_{n=1}^{N}(A(m,n)-\bar{A})(B(m,n)-\bar{B})}{\sqrt{\sum_{m=1}^{M}\sum_{n=1}^{N}(A(m,n)-\bar{A})^2 \sum_{m=1}^{M}\sum_{n=1}^{N}(B(m,n)-\bar{B})^2}} \tag{8}$$

In the formula, $\bar{A}$ and $\bar{B}$ represent the average gray value of A and B.

Then define the weights ω_1 and ω_2 of the source metal material pitting defect images A and B, namely:

$$\omega_1 = \frac{1}{2}(1 - |C(A,B)|) \tag{9}$$

$$\omega_2 = 1 - \omega_1 \tag{10}$$

This results in the weighted average fusion rule:

$$F(m,n) = \omega_1 A(m,n) + \omega_2 B(m,n) \tag{11}$$

When the simplest weighted average fusion rule is C(A, B) = 0, take $\omega_1 = \omega_2 = 0.5$.

The region fusion rule considers the variance, energy, gradient and other features of the region in the metal material pitting defect image, and carries out the region weighted fusion according to the matching degree of the features.

Select a specific fusion rule to select the components of each layer obtained by decomposition, and then perform inverse wavelet transformation, as shown in the following formula, to obtain the fusion defect image of the metal material.

$$C_{j-1}(m,n) = \frac{1}{2}\left[\sum_{k/ez} C_j(k,l)h_{m-2k}h_{n-2l} + \sum_{k,j=Z} d_j^1(m,n)h_{m-2k}g_{n-2l}\right] \tag{12}$$

In this paper, the visual signal processing of metal material pitting defect image is carried out, and the details of the image in different directions and scales are extracted The algorithm decomposes the metal material pitting defect image, obtains the low-frequency component and the high-dimensional component with multiple resolution and multiple features. Select the specific fusion rules to select the components of each layer, and then carry out the wavelet inverse transformation to complete the fusion and analysis of the metal material pitting defect visual signal. Next, through the design of metal material pitting defect recognition process, to achieve Identification of pitting defects in existing metal materials.

2.4 Design the Process of Identifying Pitting Defects in Metal Materials

The process of metal material pitting defect identification is shown in Fig. 4.

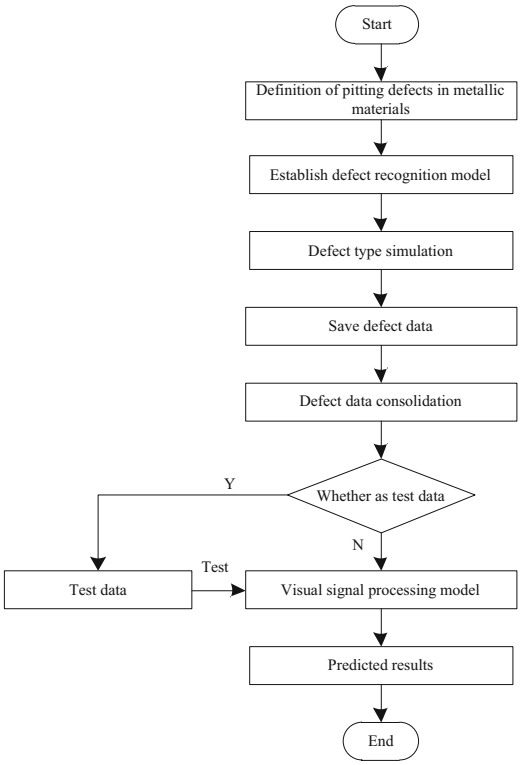

Fig. 4. Process of identifying pitting defects in metallic materials

It can be seen from Fig. 4 that the whole process of metal material pitting defect recognition is based on visual signal processing and recognition platform, which is mainly divided into two parts: visual signal processing training and test data production and application of visual signal processing for recognition, so as to realize the recognition of metal material pitting defect.

3 Experimental Study

In order to verify the effectiveness of the metal pitting defect recognition method based on visual signal processing, the following experiments are designed.

3.1 Test 1 Settings and Results

The basic situation of the first group of experiments is shown in Table 3.

Table 3. The contents of the first group of experiments

Experimental content	Parameter
Material science	Steel
Thickness	8 mm
Identification method	Visual signal processing regression
Types of pitting defects in metallic materials	Hemispherical
Simulation dimension	Three-dimensional
Data type	BY
Radius range of pitting defects in metallic Materials	1 mm–7 mm
Number of training data sets	31
Number of test data sets	3

The test object of the first set of experiments is a steel plate with an area of 460 mm × 46 mm and a thickness of 8 mm. The type of defect is a hemispherical metal material pitting defect, so the length, width and depth of the metal material pitting defect are all equal, and there is only one unknown parameter, that is, the radius of the metal material pitting defect. Therefore, the only parameter to be identified is the radius of pitting defects in metallic materials. The defect radius is between 1 mm and 7 mm, and multiple sets of defects are simulated with a step length of 0.2 mm. So the defect radius is 1 mm, 1.2 mm, 1.4 mm,…, 7 mm, 31 groups in total. Therefore, there are 31 sets of training data. In addition, the visual signal processing regression results of three sets of data are shown in Table 4.

Table 4. Prediction results of the first group of experiments

Simulation defect radius (mm)	Prediction of defect radius (mm)	Identification error
2.1	2.31887	10.04%
2.5	2.43143	2.74%
2.9	2.58893	10.72%

In terms of the amount of training data and test data, the scale of this set of experiments is small, and the types of pitting defects in metal materials are relatively simple. The maximum recognition error is about 10%.

3.2 Setup and Results of Test 2

The basic conditions of the second set of experiments are shown in Table 5.

The test object of the second set of experiments is a steel plate with a size of 460 mm × 460 mm and a thickness of 10 mm. The type of metal material pitting defect is

Table 5. The contents of the second group of experiments

Experimental content	Parameter
Material Science	Steel
Thickness	8 mm
Identification mode	Visual signal processing regression
Number of categories	8 categories
Types of pitting defects in metallic materials	Semiellipsoid
Simulation dimension	Three-dimensional
Data type	BX, BY
Radius range of pitting defects in metallic materials	1 mm–8 mm
Number of training data sets	413
Number of test data sets	32

semi-ellipsoid, so the number of metal material pitting defect parameters is three, the length, width and depth of the defect. The variation range of defect length, width and depth takes an integer value between 1 mm and 8 mm respectively, so that there are 512 groups of metal material pitting defects after permutation and combination. However, the ratio of length, width and depth of pitting corrosion defects in some metal materials is very different. For example, the length, width and depth are respectively 8 mm, 1 mm and 8 mm. Such metal material pitting defects are more like a crack than a corrosion defect. After eliminating defects with a large difference in the ratio of length, width and depth, 445 sets of simulation data were used as training and test data for visual signal processing. Among 445 sets of data, 10 sets are randomly selected as test data, so there are 413 sets of training data and 10 sets of test data. The classification results of pitting defects in metallic materials are shown in Table 6.

Table 6. Prediction results of the second group of experiments

Actual length category	Test length category	Actual width category	Test width category	Actual depth category	Test depth category	Actual depth category	Test depth category
1	2	1	1	3	5	5	5
1	1	3	3	2	2	8	7
1	1	6	7	6	6	6	6
2	2	6	6	4	3	4	3
3	4	2	2	3	4	2	2
4	4	1	2	2	4	7	7

(*continued*)

Table 6. (*continued*)

Actual length category	Test length category	Actual width category	Test width category	Actual depth category	Test depth category	Actual depth category	Test depth category
5	5	5	5	2	2	2	2
6	5	7	7	7	7	1	1
8	8	4	5	3	2	3	3
8	7	4	4	5	7	7	6

From the experimental results in Table 6, it can be seen that the prediction results of metal material pitting defect recognition obtained by this method are close to the actual results, which proves the effectiveness of the metal material pitting defect recognition method based on visual signal processing.

4 Conclusion

In this paper, a method to identify the pitting defects of metal materials based on visual signal processing is proposed. According to the distribution location of rail cracks, a model of metal materials with defects is constructed. Then, the optical signals of the pitting defects of metal materials are collected and the details of the images in different directions and scales are extracted through the signal processing process. Based on this, the image of metal material pitting defects was decomposed by Mallet algorithm, and specific fusion rules were selected to select each layer component obtained by decomposition. After inverse wavelet transformation, the visual signal fusion and analysis of metal material pitting defects were completed. Experimental results show that the recognition performance of this method is better.

Although the above research results have been achieved in this paper, there are still some deficiencies waiting for improvement, which are mainly reflected in the following aspects: the existing mimics of pitting defects of typical metal materials in the laboratory are few, and it is difficult to obtain through mechanical processing, so it is impossible to obtain rich characteristic parameters of typical defects. In the future, the pitting defect identification system can be used for feature extraction and classification of typical defects, so as to further improve the function of defect recognition.

References

1. Tam, W.C.J., Blanton, R.D.S.: LASIC: layout analysis for systematic IC-defect identification using clustering. IEEE Trans. Comput. Aided Des. Integr. Circuits Syst. **34**(8), 1278–1290 (2015)

2. Zaffuto, B.J., Conley, G.W., Connolly, G.C., et al.: Development of computer-aided radiographic inspection system (II): method of identification and categorization of welded defects. In: Sugita, Y. et al. (eds.) Proceedings of the 10th International Conference on NDE in the Nuclear and Pressure Vessel Industries, Glasgow (Scotland), 11C14 Jun. 1990. 693C699. Edited by M.J. Whittle, J.E. Doherty and K. Iida. ASM International, (1990). Vox Sanguinis, vol. 13, no. 2, pp. 77–87 (2015)
3. Chakaroun, M., Ouladsine, M., Djeziri, M., et al.: Reactive sampling for efficient defect source Identification. IEEE Trans. Semicond. Manuf. **29**(2), 104–115 (2017)
4. Sun, J.M., Liu, T., Cheng, X.Z., et al.: Nondestructive detecting metho d for metal material defects based on multimo dal signals[J]. Acta Physica Sinica **16**, 223–236 (2016)
5. Liyan, S.: Method of packaging printing defects detection based on machine vision and image processing. Bull. Sci. Technol. **34**(10), 105–108 (2018)
6. Yang, C.L.: Micro defects detection in metallic materials based on recurrence analysis of ultrasonic backscattering signal. Opt. Precis. Eng. **27**(04), 932–944 (2019)
7. Turkkahraman, D., Alper, O.M., Pehlivanoglu, S., et al.: Analysis of TPO gene in Turkish children with iodide organification defect: identification of a novel mutation. Endocrine **37**(1), 124–128 (2010)
8. Liu, S., Li, Z., Zhang, Y., Cheng, X.: Introduction of key problems in long-distance learning and training. Mobile Netw. Appl. **24**(1), 1–4 (2019)
9. Shuai, L., Weiling, B., Nianyin, Z., et al.: A fast fractal based compression for MRI images. IEEE Access **7**, 62412–62420 (2019)
10. Shuai, L., Dongye, L., Gautam, S., et al.: Overview and methods of correlation filter algorithms in object tracking. Complex Intell. Syst. **3**, 1–23 (2020) https://doi.org/10.1007/s40747-020-00161-4
11. Li, X.D., Yin, C.B., Chen, X., et al.: Simulation of infrared thermal wave detection for metal defect recognition hoisting machinery. Constr. Mach. Technol. Manage. **000**(003), 58–61 (2019)
12. Dai, X.H., Chen, H.J., Zhu, C.P.: Surface defect detection and realization of metal workpiece based on improved faster RCNN. Surf. Technol. **49**(10), 362–371 (2020)